RNA (1997), 3:89–103. Cambridge University Press. Printed in the USA.

Probing the structure of the *Escherichia coli* 10Sa RNA (tmRNA)

BRICE FELDEN,[1] HYOUTA HIMENO,[3] AKIRA MUTO,[3] JOHN P. McCUTCHEON,[2] JOHN F. ATKINS,[2] and RAYMOND F. GESTELAND[1,2]

[1]Howard Hughes Medical Institute and [2]Department of Human Genetics, University of Utah, Salt Lake City, Utah 84112, USA
[3]Department of Biology, Faculty of Science, Hirosaki University, Hirosaki 036, Japan

ABSTRACT

The conformation of the *Escherichia coli* 10Sa RNA (tmRNA) in solution was investigated using chemical and enzymatic probes. Single- and double-stranded domains were identified by hydrolysis of tmRNA in imidazole buffer and by lead(II)-induced cleavages. Ribonucleases T_1 and S_1 were used to map unpaired nucleotides and ribonuclease V_1 was used to identify paired bases or stacked nucleotides. Specific atomic positions of bases were probed with dimethylsulfate, a carbodiimide, and diethylpyrocarbonate. Covariations, identified by sequence alignment with nine other tmRNA sequences, suggest the presence of several tertiary interactions, including pseudoknots. Temperature-gradient gel electrophoresis experiments showed structural transitions of tmRNA starting around 40 °C, and enzymatic probing performed at selected temperatures revealed the progressive melting of several predicted interactions.

Based on these data, a secondary structure is proposed, containing two stems, four stem-loops, four pseudoknots, and an unstable structural domain, some connected by single-stranded A-rich sequence stretches. A tRNA-like domain, including an already reported acceptor branch, is supported by the probing data. A second structural domain encompasses the coding sequence, which extends from the top of one stem-loop to the top of another, with a 7-nt single-stranded stretch between. A third structural module containing pseudoknots connects and probably orients the tRNA-like domain and the coding sequence. Several discrepancies between the probing data and the phylogeny suggest that *E. coli* tmRNA undergoes a conformational change.

Keywords: covariation; pseudoknot; 10Sa RNA; structural probing; tmRNA

INTRODUCTION

10Sa RNA or tmRNA is a small stable RNA (Ray & Apirion, 1979) first found in *Escherichia coli* and present in many bacteria. In *E. coli*, there are about 1,000 copies per cell (Lee et al., 1978). tmRNA is encoded by the *ssrA* gene (Chauhan & Apirion, 1989; Komine & Inokuchi, 1991), and disruption of *ssrA* affects cell growth (Oh & Apirion, 1991; Komine et al., 1994). Until recently, very little was known about the function of tmRNA. Tu et al. (1995) observed that the carboxy termini of truncated *E. coli* proteins destined for degradation have identical 11-amino acid tags. Surprisingly, the last 10 residues of this peptide tag are encoded by the *E. coli ssrA* gene. tmRNAs from *E. coli* and *Bacillus subtilis* possess tRNA-like properties and can be charged in vitro with alanine (Komine et al., 1994; Ushida et al., 1994); alanine is the amino acid linking the truncated protein to the 10 amino acids encoded by tmRNA (Tu et al., 1995). Keiler et al. (1996) reported that these tags were added to polypeptides translated from mRNAs lacking a termination codon, and showed that the added 11-amino acid carboxy-terminal tag makes the protein a target for specific proteolysis. A model was proposed where charged alanyl-tmRNA rescues ribosomes stalled at the 3′ end of truncated mRNAs lacking a stop codon (Fig. 1). The tmRNA first donates its alanine to the stalled peptide chain, and then the tmRNA encoded tag is added to the carboxy terminus of the nascent polypeptide chain by cotranslational switching of the ribosome from the truncated messenger RNA to the internal sequence in tmRNA. Normal termination at the end of the terminal 10 codons allows the previously "trapped" ribosomes to recycle, and the 11-amino acid carboxy-terminal tag ensures that the aberrant protein products are de-

Reprint requests to: Raymond F. Gesteland, Howard Hughes Medical Institute, 6160 Eccles Genetics Bldg., University of Utah, Salt Lake City, Utah 84112, USA; e-mail: rayg@genetics.utah.edu.

Abbreviations: CMCT, *N*-cyclohexyl-*N*′-[2-(*N*-methyl-morpholino)-ethyl]-carbo-diimide-4-toluene sulfonate; DEPC, diethylpyrocarbonate; DMS, dimethylsulfate; IPTG, isopropyl thio-β-D-galactoside. TGGE, temperature gradient gel electrophoresis.

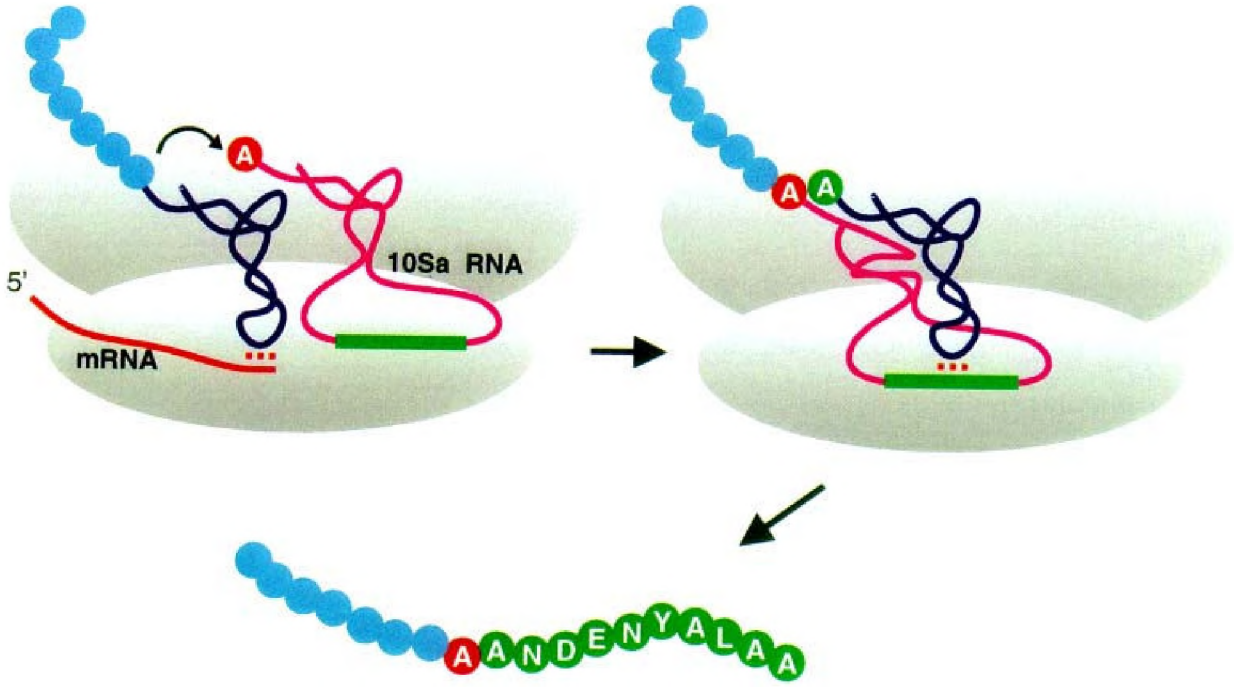

FIGURE 1. A model for the involvement of *E. coli* tmRNA in tagging truncated proteins by *trans*-translation (drawing adapted from Jentsch, 1996).

graded (Keiler et al., 1996; for reviews about the biological relevance of this unusual tagging mechanism, see Atkins & Gesteland, 1996 and Jentsch, 1996). H. Himeno, M. Sato, T. Tadaki, M. Fukushima, C. Ushida & A. Muto (unpubl. data) have shown that this tagging reaction also functions in vitro during translation of polyU, where tmRNA stimulates incorporation of the amino acid tag onto the polyphenylalanine product, presumably because the polyU lacks a termination codon (see also Muto et al., 1996).

The present work leads to a proposed secondary structure of purified *E. coli* tmRNA on the basis of covariation of sequences from different organisms and on its reactivity in solution toward enzymatic and chemical probes. This study may help explain how a single molecule can fulfill two biological functions that are usually reserved for two distinct RNA molecules, namely tRNA and mRNA. Until now, structural information was unavailable. The large size of this molecule, however, was a challenge for such an experimental approach.

RESULTS AND DISCUSSION

Analysis of biochemical data

The enzymatic and the chemical probing data (Figs. 2, 3, 4) are discussed together. Figure 2 displays results of enzymatic and imidazole probing and Figure 3 shows the lead-induced hydrolysis data. Together, these probes provide similar structural information, discriminating between single- and double-stranded domains within the tmRNA structure [S_1, lead (see below), and imidazole cleave single strands; V_1 cleaves double strands or stacked nucleotides; see Vlassov et al. (1995) for the specificity of imidazole cleavage]. Figure 4 shows the reactivities of specific atomic positions of nucleotides in *E. coli* tmRNA (both the Watson–Crick positions of nucleotides and the Hoogsteen positions of purines). After comments about Figures 2A, 3A, and 4A (top three panels), the probing data will be divided as follows: all the single- and double-stranded domains that are supported by the probing data, those that are supported only partially, and regions showing unusual probing patterns. The latter will be discussed in the light of the additional data presented in the following sections.

Representative electrophoretic patterns are presented (the mapping of the whole structure was performed with several experiments for each probe), but the full description of the sites of modification or cleavage are mapped onto the RNA sequence. The probing data have allowed discrimination between the single- and double-stranded regions within tmRNA. Figure 2A shows that the cleavage patterns generated by imidazole and ribonucleases are consistent with one another, namely that the RNA regions cleaved by imidazole correspond to regions cut by RNase S_1 (e.g., between nt A81 and A83 in Fig. 2A). Several regions that are not cleaved by imidazole are cut by RNase V_1, specific for double-stranded RNA (e.g., between nt A135 and A149 in Fig. 2). However, some ambiguities are

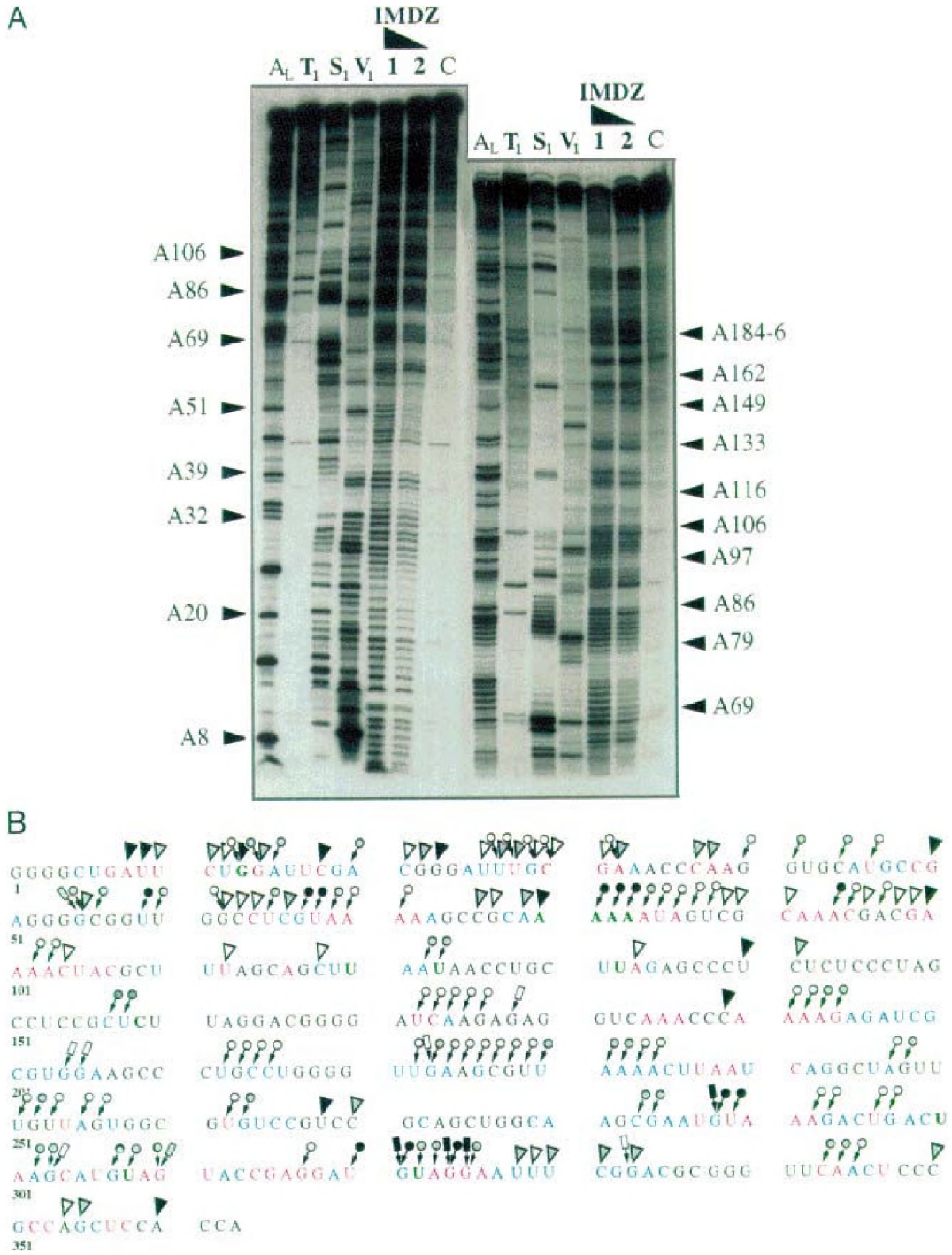

FIGURE 2. Nuclease mapping and imidazole cleavages of *E. coli* tmRNA. Top: Autoradiogram of 10% polyacrylamide gel of cleavage products of 5′-labeled RNAs. Lanes C, incubation controls; lanes 1 and 2, hydrolysis by incubation in 1.6 M and 0.8 M imidazole buffers, respectively, containing 40 mM NaCl, 1 mM EDTA, and 10 mM $MgCl_2$ for 13 h at 37 °C. Experimental conditions for nuclease mapping (performed at pH 7.5) were as follows: 0.4 units of RNase V_1, 100 units of nuclease S_1, and 6.10^{-2} units of RNAse T_1; incubation times were all 7 min at 37 °C. A range of concentration for each enzyme has been performed to define the optimal conditions for probing. Lanes A_L, RNase U_2 hydrolysis ladder. Sequencing tracks are numbered every 7 to 22 residues at A's. Bottom: Nuclease and imidazole probing data indicated on the *E. coli* tmRNA sequence described by Komine et al. (1994). Cuts induced by RNases V_1 (▷), T_1 (▭►), nuclease S_1 (○►). Intensities of cuts and cleavages are proportional to the darkness of the symbols: open, stippled, and filled for weak, medium, and strong cuts or cleavages points, respectively. Imidazole-induced cleavage points are shown using a color code: black, blue, purple, and green nucleotides correspond to uncleaved, weakly, medium, and strongly cleaved nucleotides, respectively.

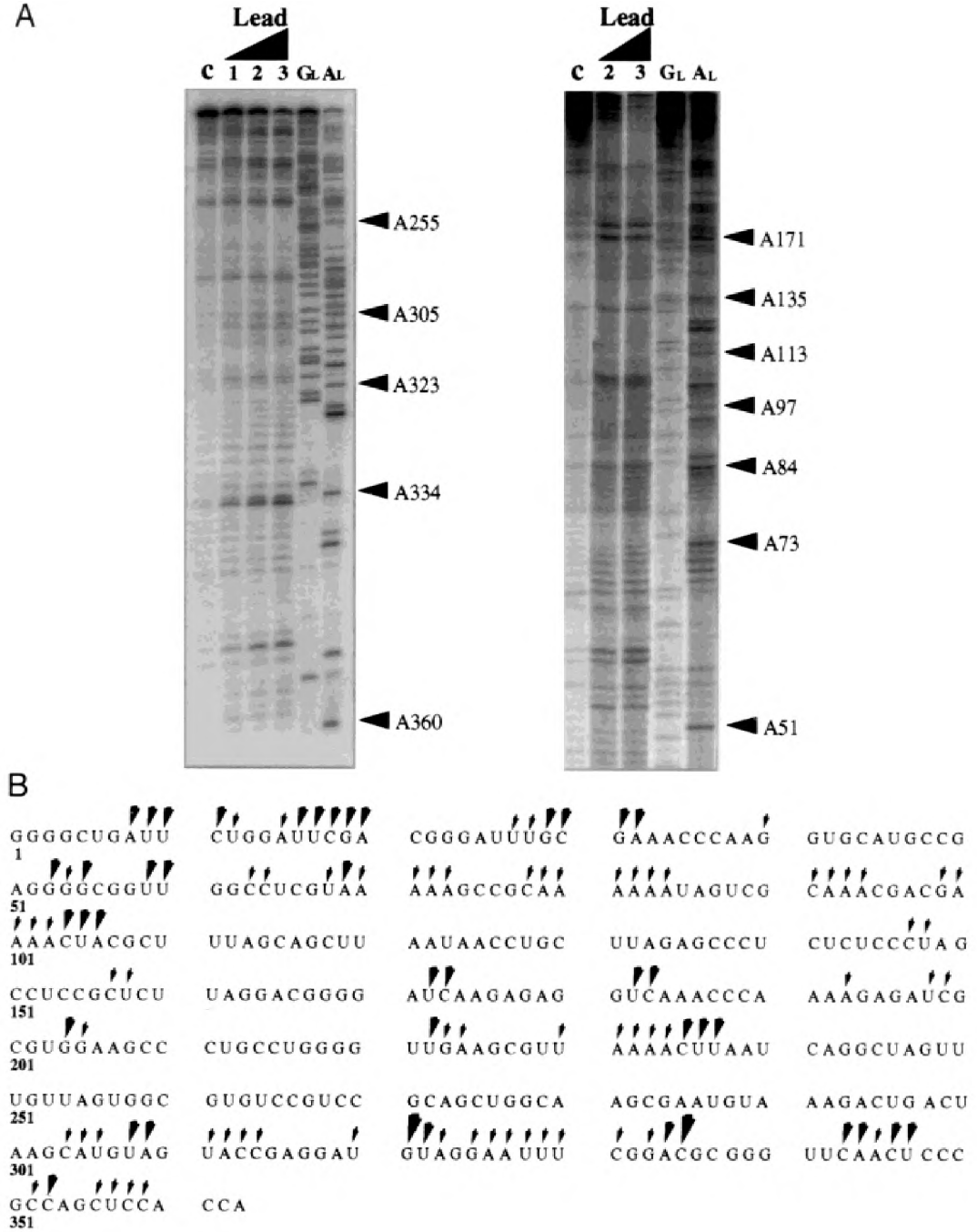

FIGURE 3. Lead acetate probing data collected on *E. coli* tmRNA. Top: Autoradiograms of 10% polyacrylamide gels of cleavage products of 3′- (top left) and 5′-labeled (top right) tmRNA. Lanes C, incubation controls; lanes 1, 2, and 3, Pb^{2+} hydrolysis by incubation in 0.7 mM, 1 mM, and 1.3 mM lead acetate (final concentration) for 5 min, respectively. Lanes G_L, RNase T_1 hydrolysis ladder. Lanes A_L, RNase U_2 hydrolysis ladder. Sequencing tracks are numbered every 10 to 50 residues. Bottom: Lead cleavages data indicated on the *E. coli* tmRNA sequence (Komine et al., 1994). Thickness of the arrowheads refers to the intensity of cleavages (weak, medium, and strong).

seen probably due to mechanistic and size differences between the enzymatic and chemical probes. Several V_1 and S_1 cuts do not correspond precisely to the locations found with imidazole cleavage—the sites are shifted by one or more nucleotide(s) (e.g., between nt G77 and U88 in Fig. 2). Differences in size and cleavage mechanisms between these probes presumably account, at least in part, for these findings. Figure 3A shows lead(II)-induced cleavages using two to three different lead concentrations. Only a few sites are cleaved to give products that are not already present in the control sample without lead (Fig. 3). The bands that are lead-specific have greater intensity with increasing lead concentration. Figure 4A shows two ex-

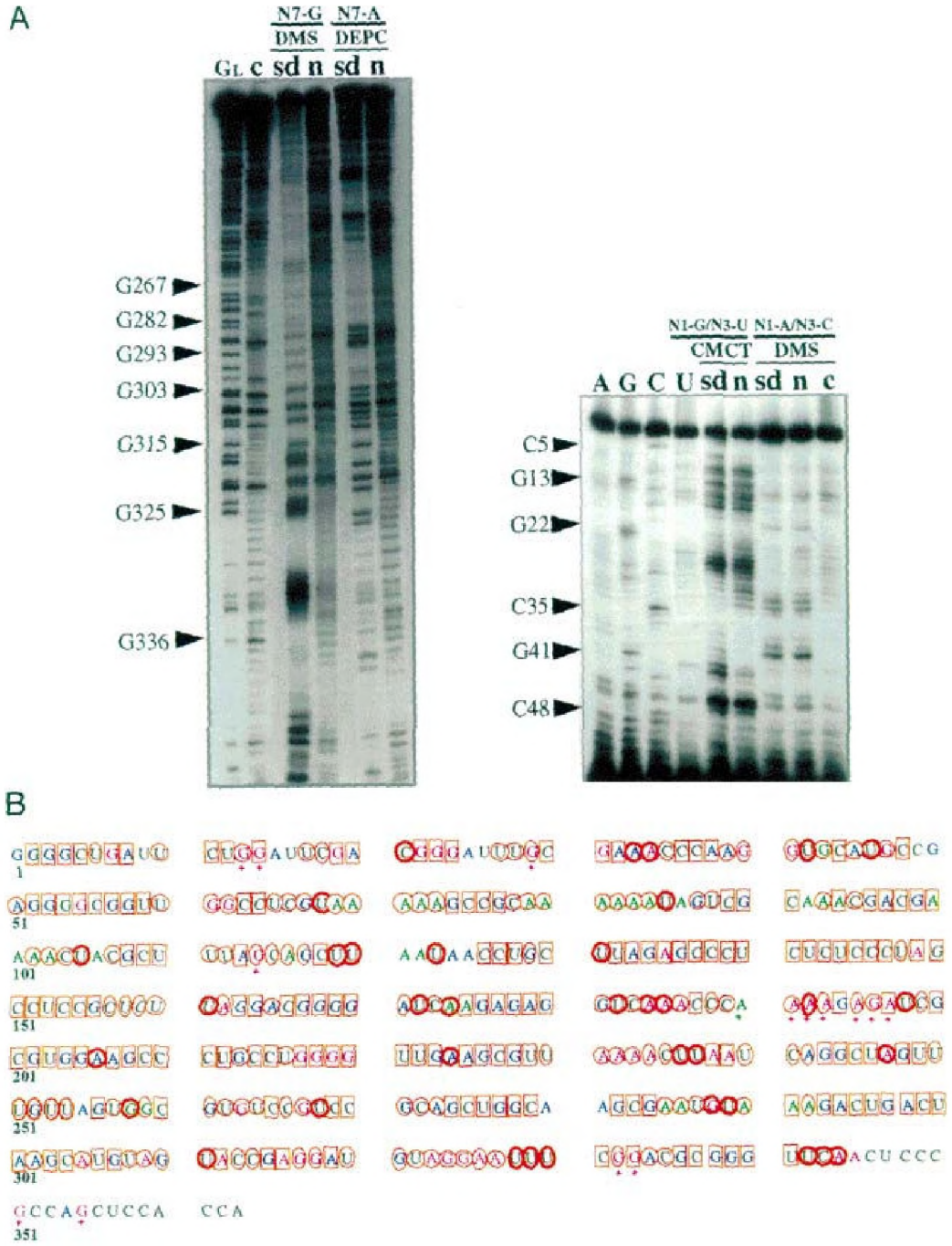

FIGURE 4. Mapping data of Hoogsteen and Watson–Crick positions of each nucleotide of *E. coli* tmRNA. Top: Mapping of N-7 positions in the purines of *E. coli* tmRNA by DMS, and by DEPC by the direct method (top left) and of Watson–Crick positions by DMS and CMCT using primer extension (oligonucleotide 5) followed by reverse transcription (top right). Autoradiograms of 8% polyacrylamide gels of cleavage products of 3′-labeled RNAs (top left), and of extended 5′-labeled DNA oligonucleotides (top right). Lanes C, incubation controls; lanes N, probing under native conditions. Lanes SD, probing under semi-denaturing conditions. Lane G_L, guanosine ladder. Lanes A, G, C, and U are sequencing ladders generated in the presence of ddTTP, ddCTP, ddGTP and ddATP. Sequencing tracks are numbered every 10 to 15 G residue. Note that the control lane in the top left panel contains several bands, inherent to the method of detection of the modified purines. Indeed, after chemical modification of the accessible purines, several chemical treatments are required to reveal the modified positions, thus accounting for at least some of the degradations observed in the control lane (bottom). Chemical reactivities are indicated on the *E. coli* tmRNA sequence (Komine et al., 1994). Reactivities under native conditions (○), under semi-denaturing conditions but not in native conditions (**O**), or no reactivities under both native and semi-denaturing conditions (□) of adenines (atoms N-1), cytosines (atoms N-3), guanines (atoms N-1), and uridines (atoms N-3), indicated in orange. Strong and moderate reactivities are denoted by bold and thin symbols, respectively. Chemical reactivities of adenines and guanines (atoms N-7) are color coded: green under native conditions, pink under semi-denaturing conditions, or dark blue only when the RNA structure is denatured. Strong reactivities are denoted by a (+) below the nucleotide. Some nucleotides could not be tested because of degradation. Watson–Crick reactivities of the last 19 nt located at the very 3′ end could not be tested (corresponding to the site of annealing of the first complementary oligonucleotide).

amples of data obtained when probing both the N-7 positions of purines using DMS and DEPC (top left panel) and the Watson–Crick (N-1 positions of adenines and guanines, N-3 positions of cytosines and uridines) positions of nucleotides using a carbodiimide and a different revelation method for DMS (see the Materials and methods). For the latter approach, five oligonucleotides were needed to cover the entire tmRNA sequence, and the results obtained on the 5′ end of the molecule are shown (top right panel).

Taken together, the enzymatic and chemical probing data indicate that U68–A73, A81–A84, A101–C107 (despite a small V_1 cut), U172–A174, A191–A193, U230–U237, U320–A326, and U342–U347 are single-stranded. These regions of the RNA are cut by nuclease S_1, by lead, and by imidazole. Both their Watson–Crick and Hoogsteen positions are fully reactive in native conditions (in the presence of magnesium), or to a lesser extent in semi-denaturing conditions (in the presence of 1 mM EDTA) (Figs. 2B, 3B, 4B). Three regions, A92–A93, G181–A186, and U198–C199, appear to be single-stranded, but are not cut by S_1, perhaps due to inaccessibility of the bulky enzyme. Three regions of *E. coli* tmRNA, namely U119–U123, U262–G263, and A285–A292, appear to be single-stranded according to the probing data, except for that obtained from lead cleavage. Unlike other single-stranded specific probes, the lead-induced hydrolysis of single-stranded RNA sequences requires coordination of lead to neighbor sequences, as well as particular geometry of the targeted RNA sequences (Werner et al., 1976; Brown et al., 1983). Perhaps these three regions of tmRNA do not fulfill both the conformational and the neighboring requirements to be cleaved by lead despite being single-stranded.

The probing data suggest that G1–G7, G74–G77, C89–G90, G108–U110, A113–C118, C126–C130, A133–C146, A149–G156, C166–G170, A177–G180, G200–U203, A207–C211, G217–U221, A225–U229, G243–C245, G274–G282, and G336–U341 appear double-stranded. These sequence stretches are not cut by RNase S_1, and several are cut by V_1. They are not, or are only weakly, cut by imidazole (Fig. 2) or by lead (Fig. 3). Both the Watson–Crick positions of these nucleotides, as well as the Hoogsteen positions of purines, are protected from modification, although a few are accessible to some extent in semi-denaturing conditions (Fig. 4). Some of the probing data, especially that from DMS and CMCT, indicate that G293–A298, U328–C331, and C353–C359 are double-stranded, except for minor S_1, lead, or imidazole cuts. If correct, these paired portions might be breathing somewhat in solution, but the data is ambiguous. An unusual probing pattern was observed between A8 and U33 (see the presence of both V_1 and S_1 cuts at several identical positions in Fig. 2A), as if this domain breathes considerably in solution (the other probing results support this idea). The few other regions of tmRNA that are not included in that analysis will be discussed in the next section, because additional data were required to define their conformation in solution.

Alignment of tmRNA sequences

Because *E. coli* tmRNA is a large molecule (363 nt), many secondary structure models are possible even if the probing data considerably restrict the number of realistic solutions. To start on a solid basis, a sequence alignment was performed to identify putative interactions that would be supported by covariation. Figure 5 shows an alignment of nine predicted tmRNA sequences derived from their gene sequences, with that from *E. coli* (Chauhan & Apirion, 1989). Although there is no evidence, it may be that tmRNA sequences are posttranscriptionally modified. If this caution is correct, the tmRNA sequences shown need correction. The tmRNA sequences are from *Haemophilus influenzae* (Fleischmann et al., 1995), *Vibrio cholerae* (Kovach, 1995), *Alcaligenes eutrophus* (Brown et al., 1990), the incomplete sequence of *Thermus thermophilus* (H. Vornlocher & M. Sprinzl, unpubl., Genbank accession no. Z48001), the incomplete sequence of *Dichelobacter nodosus* (V. Haring, C.L. Wright, S.J. Billington, A.S. Huggins, M.E. Katz, & J.I. Rood, unpubl., Genbank accession no. U20246), *B. subtilis* (Ushida et al., 1994), *Mycoplasma capricolum* (Ushida et al., 1994)), *Mycoplasma genitalium* (Fraser et al., 1995), and *Mycobacterium tuberculosis* (Tyagi & Kinger, 1992). The covariations between the

FIGURE 5. Sequence alignments of 10 tmRNA sequences emphasizing several interactions supported by covariations. The tmRNA sequence of *E. coli* is used as a reference (underlined) for comparisons with the deduced RNA sequences from the tmRNA genes of *H. influenzae*, *V. cholerae*, *A. eutrophus*, *T. thermophilus* (incomplete), *B. subtilis*, *D. nodosus*, *M. capricolum*, *M. genitalium*, and *M. tuberculosis*. The color boxes indicate the base pairings supported by covariations (helices H1, H2, and H6 and pseudoknots PK1, PK2, PK3, and PK4), and the nonboxed colored regions indicate several possible base paired domains weakly or not supported by covariations (helices H3, H4, and H5 and domain R1). The circled nucleotides (shaded boxes) indicate covariations and the underlined nucleotides represent noncanonical base pairs or mismatches. G-C, A-U, and G-U base pairs are allowed. Dashed lines depict the missing sequences. Nucleotides shown in italics and flanked by thin lines are not aligned because no obvious alignment was found, and even alternate foldings as compared to the *E. coli* sequence are proposed (e.g., the possible helices shown in pink for *D. nodosus*, *M. genitalium*, or *M. tuberculosis*, instead of PK4). Note that R1 and H5 are shown in dashed lines because their phylogenic support is weak. The numbering is shown on the *E. coli* tmRNA sequence.

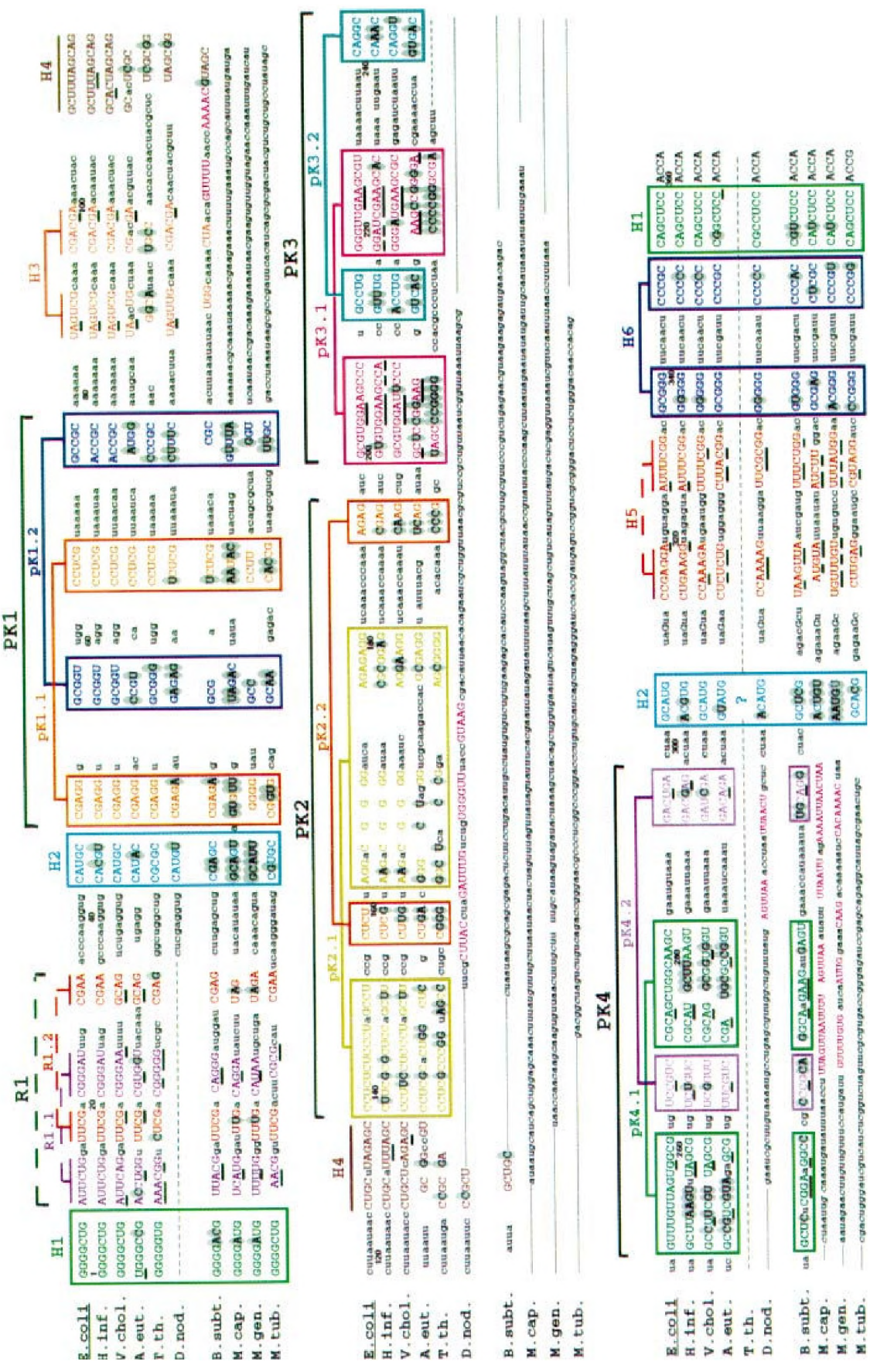
R1
R1.1
R1.2
PK1
PK1.1
PK1.2
H1
H2
H3
H4
PK2
PK2.1
PK2.2
PK3
PK3.1
PK3.2
PK4
PK4.1
PK4.2
H5
H6
E.coli
H.inf.
V.chol.
A.eut.
T.th.
D.nod.
B.subt.
M.cap.
M.gen.
M.tub.

sequences support the existence of three helices (H1, H2, and H6) and four pseudoknots (PK1, PK2, PK3, and PK4), which are boxed using a color code in Figure 5 (pseudoknots are abbreviated PK, e.g., PK1, and their constituent stems are pK plus a number indicating the first or second stem, e.g., pK1.1). Three other helices (H3, H4, and H5) and one paired region (R1) are supported to a lesser extent, requiring acceptance of several noncanonical base pairs or mismatches (shown as underlined nucleotides in Fig. 5). In *T. thermophilus*, the only thermophilic organism included in the sequence alignment, several covariations are found that would increase the stability of the proposed interactions (three G-C in pK2.2 and six G-C in pK3.1).

The proposed interactions will be described, working from the 5′ to the 3′ end of the molecule. Helix H1 mimics a tRNA acceptor stem (Komine et al., 1994; Ushida et al., 1994), and is supported by the presence of five covariations, as well as by most of the probing data (see Figs. 2, 3, 4; note that the Watson–Crick positions of nucleotides in the 3′ strand of the stem have not been probed because of annealing of the DNA probe used for detection). Consequently, the 5′ and 3′ ends of tmRNA are base paired, which may provide protection from degradation by exonucleases, as well as being important for aminoacylation.

The region designated R1 in Figure 5 will be considered next. It is shown in one possible form, a pseudoknot, in dashed lines. This folding is not well supported by covariations (see the underlined nucleotides). One of the alternate foldings of R1 includes two stem-loops (U12–G14 with U17–G19, and G22–U27 with A32–C37, with a noncanonical base pair, A25–A34, or an internal bulge). If either the pseudoknot or the above alternate pairing forms, it is likely to be unstable, as already introduced in the previous section (both V_1 and S_1 cuts, as well as lead cleavages, occur between A8 and A32). If the pseudoknot forms, the instability might arise from constraints imposed by a loop 2 of only 3 nt in the *E. coli* sequence (U27–G29) [In pseudoknots, loop 1 crosses the deep, narrow groove, and loop 2 crosses the shallow, wide groove (ten Dam et al., 1992)]. In the following sections, R1 will be discussed as either a pseudoknot or in terms of the above alternate folding.

A proposed long-range interaction involves helix H2 (boxed blue in Fig. 5). Like H1, it involves 5′ and 3′ parts of the molecule. H2 has been identified on the basis of 16 covariations, but, surprisingly, some of the probing data argues against it (two S_1 cuts in both strands of the proposed stem, and the Watson–Crick positions of A45, U46, G47, and A305 are reactive under native conditions). One possible explanation is that H2 is not present or at least unstable on initial contact with the ribosome, but a subsequent rearrangement involves the formation of H2.

PK1 is supported by both phylogeny (8 covariations in pK1.1 and 12 covariations in pK1.2) and to a significant extent by the probing data. S_1 cuts and lead cleavages are located mainly in the connecting loops, although some S_1 cuts in one strand of each "stem" are observed. The two predicted stems are cut by RNAse V_1 and both the Watson–Crick and the Hoogsteen positions of most nucleotides of the stems are protected, but the probing data suggests that stem pK1.1 is unstable.

Two stem-loops, H3 and H4, that contain the coding sequence (see below) are proposed. But, according to the sequence alignment, only two covariations for H3 and 5 for H4 are found. The probing data, however, support these two stem-loops. In *B. subtilis*, there is the potential for three stem-loops to form. The limited number of covariations in H3 and H4 may be linked to the presence of the coding sequence, thus restricting the sequence variations.

The existence of PK2 is supported by 17 covariations for pK2.1, and by 8 covariations for pK2.2. The internal bulge in the 3′-strand of pK2.1 (A171–A174) is supported by the probing data (S_1, lead, and imidazole cleave U172 and C173; S_1 and imidazole cut A174, whereas the flanking sequences are protected from being modified). The predicted loop 2 of PK2 (U182–A192) is single-stranded according to the probing data, but, surprisingly, the proposed loop 1 (C154–G156) is protected against modifications or cleavages by all the probes, thus arguing against it being single-stranded.

PK3 is also supported by phylogeny (12 covariations for pK3.1 and 6 for pK3.2). One of the proposed stems, pK3.1, has three tandem G-A pairs near the middle of the stem, a prediction supported by the probing data. Despite a few small S_1 cuts between G213 and C215, the probing data and sequence alignment (six covariations) support the existence of pK3.2. Moreover, the predicted loop 1 (U212) and loop 2 (U230–U240) are single-stranded according to the probing data (Figs. 2–4).

PK4 is supported by 15 covariations for pK4.1, and by 5 covariations for pK4.2, but 15 noncanonical base pairs or mismatches are seen within the two stems (underlined nucleotides in Fig. 5). Both connecting loops 1 and 2 are single-stranded according to the probing data, but one strand of "stem" pK4.1, U251–G256, has S_1 cuts in a region that is also accessible to the chemical probes (in semi-denaturing conditions).

Stem-loop H5 is proposed on the basis of the probing data (V_1 cuts between U328 and C331 and strong S_1 and T_1 cuts occur in the loop U320–A326), but is not supported by phylogeny (20 noncanonical base pairs or mismatches are required to maintain the stem in the various sequences). Helix H6 is supported by seven covariations and by the probing data (the Watson–Crick positions of nucleotides in the 3′ strand of the stem have not been probed because of annealing of the

DNA probe used for detection). Probing data indicate that U341–U347 is single-stranded.

The tmRNA sequences deviating most from that of *E. coli*, namely *D. nodosus*, *B. subtilis*, *M. capricolum*, *M. genitalium*, and *M. tuberculosis*, have not been aligned in at least the center part of the sequence because of their weak similarities to their *E. coli* counterpart. However, several stable stems, depicted in pink in Figure 5, are proposed, and they deviate from the overall sequence alignment. It is likely that these tmRNAs may have different secondary structures.

Structural transitions of the *E. coli* tmRNA

Conformational transitions of nucleic acids, and especially RNAs, between an ordered, native structure and a disordered, denatured state, can be induced by changes in temperature and monitored using temperature-gradient gel electrophoresis (Rausenbaum & Riesner, 1987). Structural transitions are seen as abrupt changes in electrophoretic mobility at specific temperatures. Figure 6 depicts the result of a TGGE experiment, between 7 °C and 95 °C, with 3′ end-labeled *E. coli* tmRNA. As expected from the sequence alignment and probing data, several transitions from a fast-moving to slower-migrating bands are observed. Because the transitions are discontinuous, dissociation processes are mostly irreversible under the conditions of electrophoresis. The strongest retardation occurs around 40 °C (between segments 2 and 3 in Fig. 6), which may correspond to the disruption of at least one long-range interaction. Weaker ones are seen between 42 °C and 55 °C (segments 3–6 in Fig. 6), affecting to a lesser extent the folding of the molecule. A smear caused by RNA degradation is present between 60 °C and 95 °C. Several bands are observed between 7 °C and 35 °C, suggesting the presence of several conformations of tmRNA at low temperatures (segment 1 in Fig. 6). Interestingly, it seems that, at low temperatures and even at 37 °C, a diffuse band is observed (in contrast to the sharper band at higher temperatures), suggesting the existence of more than one conformation of tmRNA, perhaps accounting for the conflicting probing pattern observed at specific positions within the RNA structure.

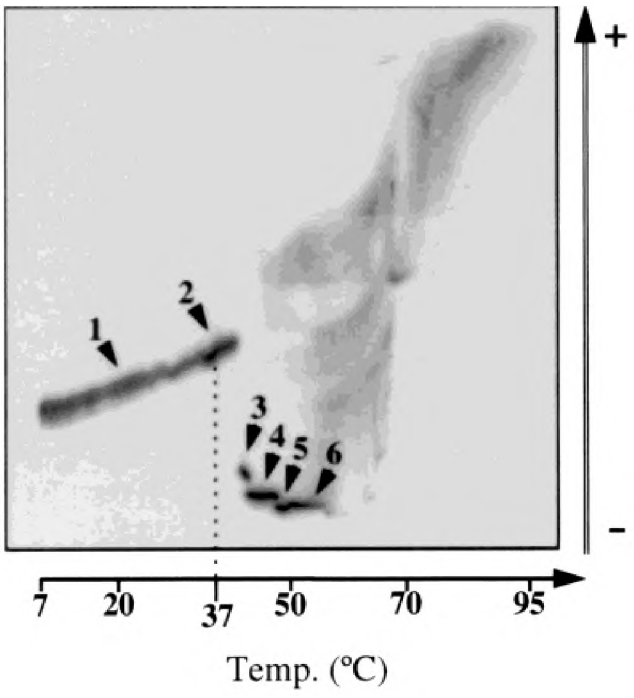

FIGURE 6. Analysis by TGGE of the *E. coli* tmRNA. Autoradiogram of a native 5% polyacrylamide gel containing 5 mM $MgCl_2$. Both the directions of migration during electrophoresis, as well as the temperature gradient (between 7 and 95 °C), are indicated. Electrophoresis of 3′-labeled tmRNAs in the presence of the temperature gradient was conducted at 300 V for 150 min. Numbers (1–6) correspond to the regions of interest discussed in the text, and these temperatures were selected for enzymatic probing. Note the large retardation of migration around 40 °C, as well as the weaker retardations at higher temperatures.

To identify structural elements within tmRNA that are melted progressively with increasing temperatures, enzymatic probing experiments were performed at five temperatures (20 °C, 37 °C, 42 °C, 46 °C, and 50 °C), selected on the basis of the main structural transitions (segments 1–6 in Fig. 6). Figure 7 illustrates the result obtained at the 5′ end (right panel) and 3′ end (left panel) of tmRNA. Near both ends of the molecule and only at 20 °C, a conflicting probing pattern has been observed. Both single- and double-stranded specific nucleases cut at similar locations (e.g., S_1 cuts between C348 and C352 and V_1 cuts at C350, both S_1 and V_1 cut at A20 and between G332 and C335), perhaps reflecting the presence of more than one conformation at low temperatures. This result is compatible with the presence of more than one band, as evidenced by TGGE (Fig. 6). We cannot rule out, however, a decrease in specificity of the enzymatic cleavages at low temperature. Surprisingly, at 20 °C, only a small fraction of the molecules possesses a probing pattern compatible with the presence of a tRNA-like structure (between U320 and A354, left panel), whereas, at higher temperature, the enzymatic cleavages are more defined, supporting the existence of a T-stem (H6), a T-loop, and even an anticodon stem-loop (H5) (discussed in the next sections).

Concerning the structural transition between 37 °C and 42 °C (between segments 2 and 3 in Fig. 6), the major differences depicted by the probing experiments have been found at the 5′ end of the molecule (Fig. 7, right panel). R1, H2, PK1, and, to a lesser extent, H3, seem partially, or even entirely, unfolded at 42 °C. Strong S_1 cuts occur between U9 and G19, U26 and C30, A32 and C38–G40, indicating that the folding of R1, already unstable at 37 °C, becomes mostly single-stranded at 42 °C, despite the retention of V_1 cuts between A8 and G13. Unfortunately, this additional data is insufficient to distinguish between the two putative secondary structures for R1 considered above. At 42 °C, the S_1

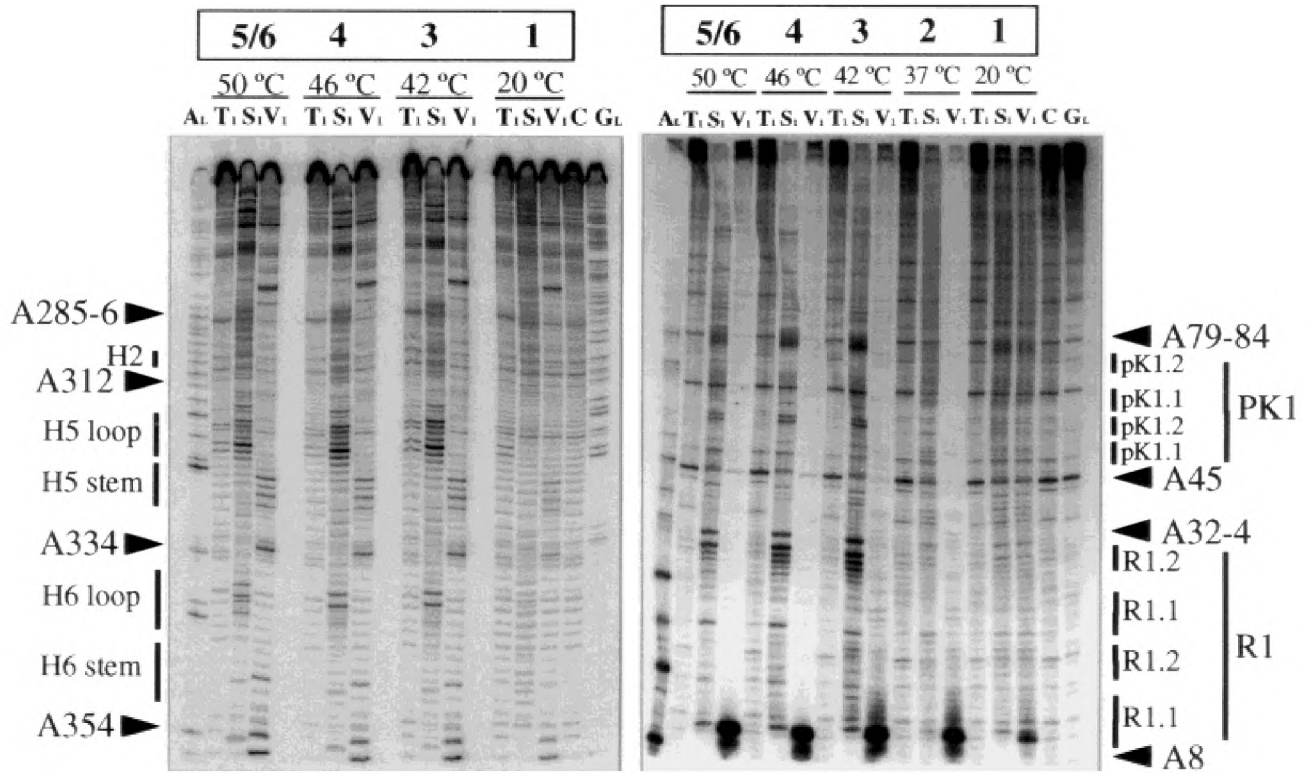

FIGURE 7. Nuclease mapping of *E. coli* tmRNA at selected temperatures. 20 °C, 37 °C, 42 °C, 46 °C, and 50 °C were choosen according to the results obtained by TGGE. Autoradiograms of 8% polyacrylamide gels of cleavage products of 3′-labeled (left) and 5′-labeled (right) RNAs. Lanes C, incubation controls. Experimental conditions were as follows: 0.3 units of V_1, 50 units of S_1, and 6.10^{-2} units of T_1; the incubation times were 7 min at the selected temperatures. Lanes A_L, RNase U_2 hydrolysis ladder. Lanes G_L, RNase T_1 hydrolysis ladder. Sequencing tracks are numbered at a few adenosines, and five secondary structural elements of tmRNA (R1, PK1, H2, H5, and H6) showing significant variations of their probing pattern when the temperature increases, despite a high background in the control lane, are indicated. Changes in band intensity have been scored using a phosphorimager.

cuts at G303 and at G307 are enhanced, indicating that H2, already unstable at 37 °C, melts at 42 °C. Nucleotides A51, C56–G57, and U60 are cut by nuclease S_1, suggesting that the two stems of PK1 also melt. S_1 cuts become stronger between A92 and A94 and at A97, indicating that H3 breathes more at 42 °C than at 37 °C. It seems likely that the strong gel retardation observed on TGGE between 37 °C and 42 °C comes from the melting of the long-range interaction H2, perhaps inducing the melting of R1, PK1, and H3.

As could be anticipated from the TGGE experiment, more subtle differences have been observed between 42 and 46 °C and between 46 and 50 °C. Between 42 and 46 °C, several V_1 cuts at the 5′ end of the molecule disappear (e.g., between U10 and G14, C21 and G23, and at G50), indicating that, at 46 °C, both R1 and pK1.1 are totally unfolded. Interestingly, strong S_1 cuts occur between G282 and C283, suggesting that one side of pK4.1 is melted, which may correspond to the small retardation observed between segments 3 and 4 in Figure 6. Between 46 °C and 50 °C, strong S_1 cuts occur at C295 and U296, suggesting that pK4.2 is unstable at 50 °C. Consequently, at 50 °C, both stems of PK4 are destabilized. PK4 is connected to the 5′ side of the structure via H2. Because H2 is already melted at 42 °C, it could be anticipated that PK4 is no longer tightly connected to the overall RNA structure, and becomes more susceptible to unfolding at higher temperatures. At 50 °C, the probing pattern of both loops H5 and H6 is changed slightly compared to that observed at lower temperatures (Fig. 7, left panel), probably due to changes in the geometry and stability of both loops. We cannot exclude, however, a deleterious effect on the specificity of enzymatic cleavages when increasing the temperature to 50 °C.

Proposal for a secondary structure

A proposed secondary structure model for *E. coli* tmRNA is shown in Figures 8 and 9. Figure 8 summarizes the probing data testing single- and double-stranded regions of tmRNA, and Figure 9 the reactivity of Watson–Crick and Hoogsteen positions of most nucleotides. Structural elements H1, H3, H4, H5, H6, pK2.1, and both stems of PK1, PK3, and PK4 are supported by the data collected. Elements H2 and pK2.2 are questionable by probing, but supported robustly by covariations. Element R1 is drawn as a pseudoknot,

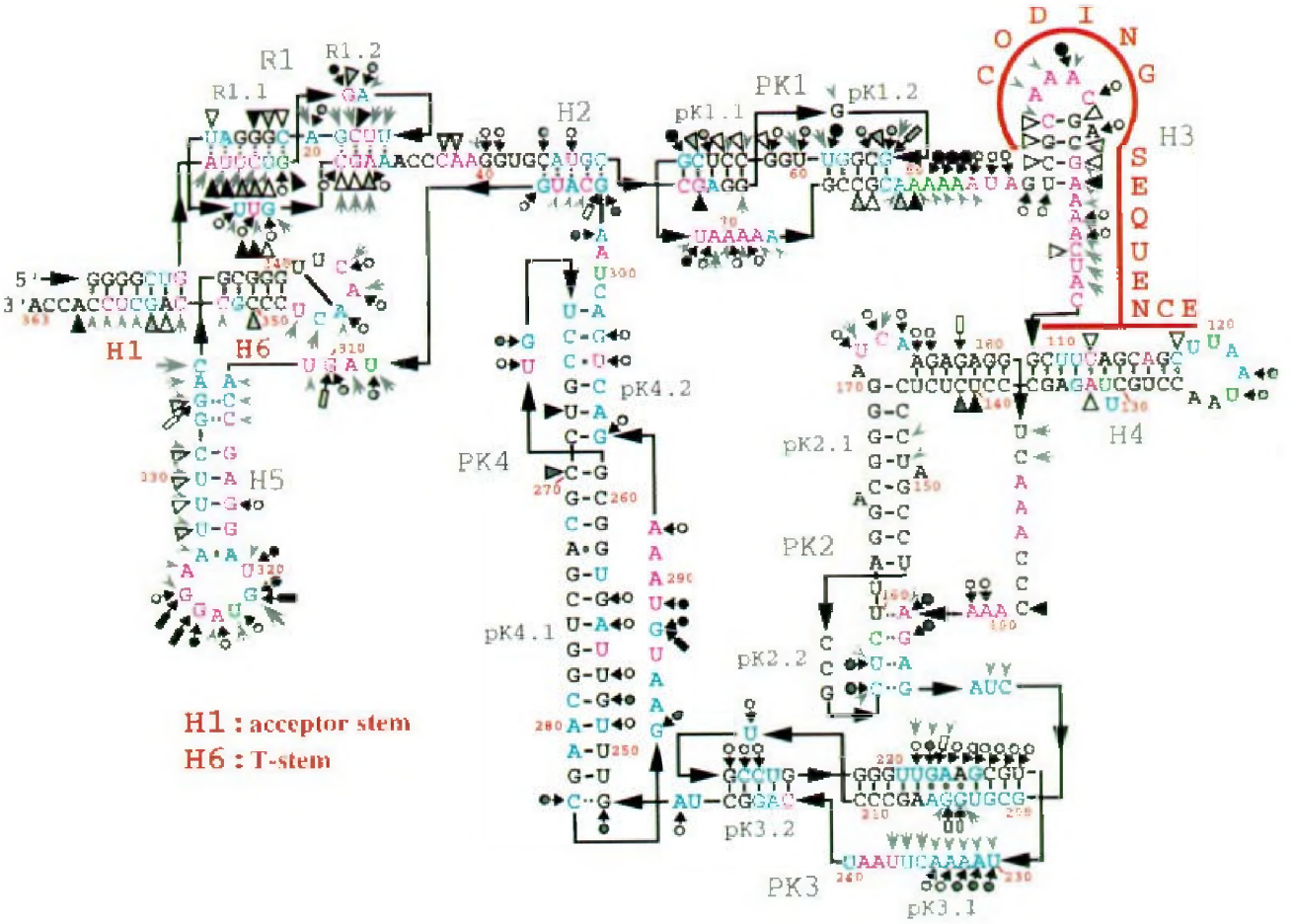

FIGURE 8. Secondary structure model for *E. coli* tmRNA showing part of the probing results. The color code and symbols for cleavages with V_1, T_1, S_1, lead acetate, and imidazole are similar to that of Figures 2B and 3B. Black arrows follow the sequence from the 5′ to the 3′ ends of the molecule, with numbering of residues from the 5′ terminus (indicated in red). Thin lines are canonical base pairs, small circles are the proposed noncanonical base pairs, or mismatches, and dashed lines are only possible base pairs according to the present data. Note that H1 and H6 (in red) are proposed to be the analogues of an acceptor arm and of a T stem-loop, respectively. The coding sequence is indicated also in red lines (between G90 and U119).

but at least one alternate form could fit the data equally well (or poorly!). Many of these structural domains are connected by single-stranded links of variable lengths (A34–G43 between R1 and H2, A79–G87 between PK1 and H3, A101–C107 between H3 and H4, A197–C199 between PK2 and PK3, U246–A247 between PK3 and PK4, C299–A302 between PK4 and H2, and U308–A312 between H2 and H5). However, in some cases, there is no connecting nucleotides (between H1 and R1.1, H2 and pK1.1, H4 and pK2.1, and H6 and H1). In general, the probing data support the existence of these single-stranded connectors (Figs. 8, 9), with one exception—the link between R1 and H2 (there are two V_1 cuts at C37–A38, and the Watson–Crick positions of C36–A38 are protected from modification). The putative double-stranded nature of part of this connecting sequence fits better with the alternate structure for R1 (but the overall probing data do not). An internal bulge within pK2.1 (A171–A174) is supported by the probing data, and is variable in sequence and length between the species (2–12 nt). Most of the connecting loops of the proposed pseudoknots appear single-stranded from probing experiments (e.g., between U68 and A73 for PK1, U230 and U240 for PK3, or G284 and A292 for PK4). However, there are exceptions (there is a strong V_1 cut at C189, and the Watson–Crick positions of nt C154–G156 are protected. In addition, the "stem" pK2.2 is cleaved on both sides by S_1). At least the V_1 cut could be rationalized by invoking the involvement of additional long-range interactions between the proposed single-stranded region and other parts of the molecule. However, unless the "stem" pK2.2, which only comprises four base pairs, is unstable in solution, the probing data are difficult to reconcile with the proposed structure. The contrast between the inferences from the probing data and covariation is discussed in the next section.

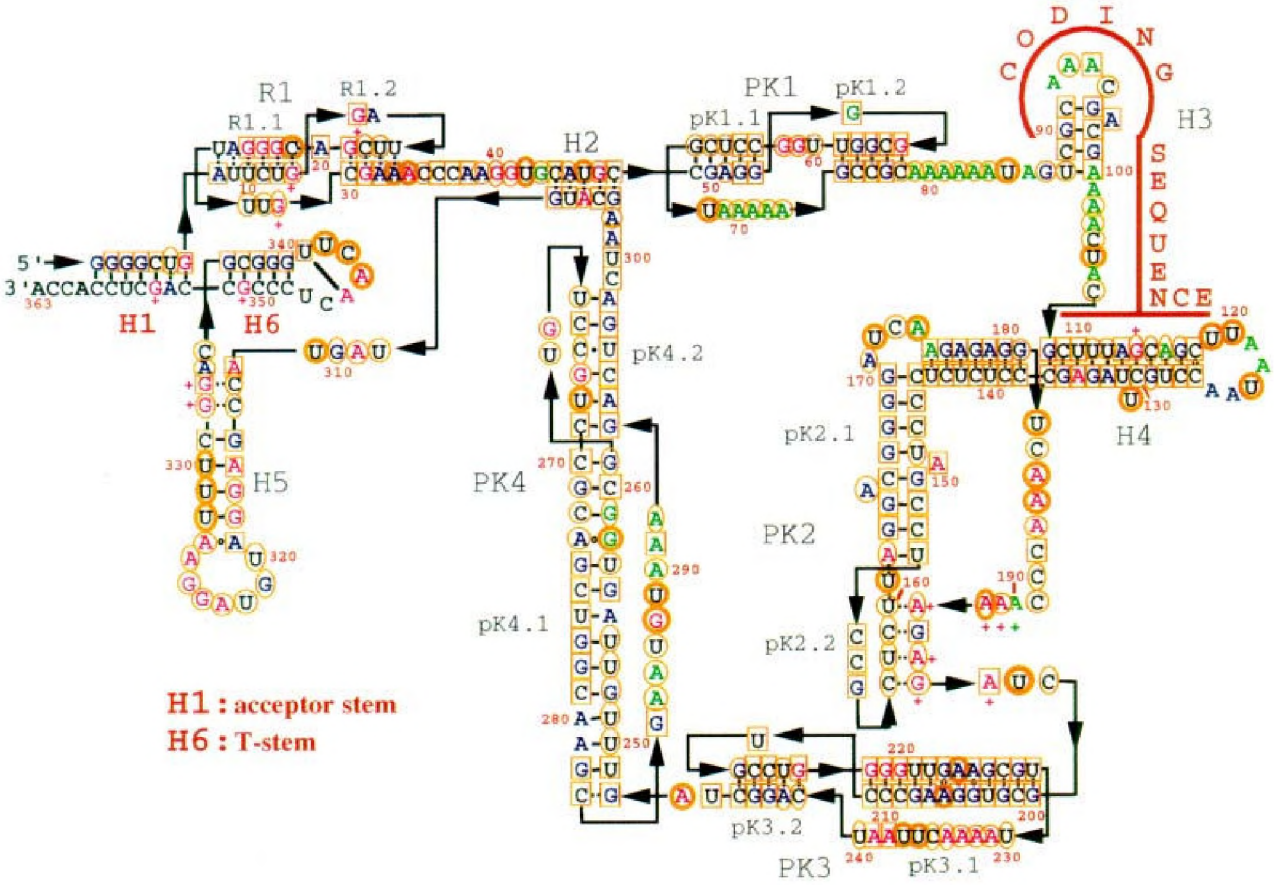

FIGURE 9. Secondary structure model for *E. coli* tmRNA showing the probing results with DMS, CMCT, and DEPC under native or semi-denaturing conditions. Color code and symbols used are similar to that of Figure 4B. Bases where no or only partial information is provided were not, or were only partially, determinable. Other indications provided are identical to Figure 8.

Structure–function relationships and biological implications

tmRNA has a complicated role. It must fit into the ribosomal A site in spite of its bulky, at least 300 nt, internal sequence. After donation of its alanine to the growing chain, it allows the ribosome access to an internal portion of the loop. How does the A site accommodate this large structure and how is access accomplished? It seems plausible that tmRNA might undergo a conformational change during the transition from tRNA to mRNA. If so, then covariation of nucleotides among the various sequences might reflect either of the two conformations, because it only represents a functionally conserved base pair. Probing experiments as performed here only access the tmRNA as it exists in solution, and not a molecule that might be induced to a different form by interaction with a ribosome, for instance. Proposed structures H2 and pK2.2 are implied by covariation, but not supported by probing, and might then represent features of a second, functional conformation not present in the molecules studied in solution. Preliminary footprinting experiments of tmRNA with the ribosome are consistent with this suggestion, because the probing pattern of H2 and of loop 2 of PK2 (as well as other parts of tmRNA) varies in the presence of ribosome (to be published). On the other hand, if the structure studied here is the crucial one before the hypothetical change, one might expect that all probing inferences would be supported by covariation, which is clearly not the case. However, some sequences might be so conserved that no or only a few variations are tolerated (e.g., H3). Despite the complexity and imponderables of an initial probing study, the combination of probing and covariation together strongly support some structural features, e.g., the pseudoknots PK3 and PK4.

It is not clear that the tmRNA as probed is the crucial initial structure—it is devoid of proteins and was analyzed in only a limited set of ionic conditions, without polyamines. Some folded domains may only be stabilized by interaction with proteins (such as EF-Tu, but this interaction is not known) or ribosomes. Probing data for R1 and PK1 are consistent with breathing of the structure in solution, and these domains might be stabilized in vivo. The recognition element for amino-

acylation with alanine is resident in this free molecule, but, at least in alanine tRNA, this is simple and localized to the acceptor stem (Francklyn & Schimmel, 1989). It has been proposed that tmRNA has more extensive mimicry with tRNA than would be required for aminoacylation (Felden et al., 1996a). Presumably, these added features are important for interaction with the ribosomal A site. However, there is no obvious need for an anticodon stem-loop according to the current model, because alanine is donated to the growing chain without direction by an mRNA.

The reported (Komine et al., 1994; Ushida et al., 1994) partial structural mimicry with canonical tRNAs, encompassing an aminoacylatable acceptor branch (an acceptor stem H1 and a T-stem H6), is supported. However, several weak lead-induced cleavages on one strand of H1 suggest that the acceptor stem is breathing. The probing data also support the presence of the analogue of a T-loop found in canonical tRNAs, with the proposed base pair U341–A345 perhaps mimicking a reverse-Hoogsteen base pair (Figs. 8 and 9), as suggested (Felden et al., 1996a). Probing suggests that helix 5 (H5), with at least five base pairs in the stem (one is an A-A noncanonical base pair) and a 7-nt loop, may mimic an "anticodon stem-loop," as proposed (Felden et al., 1996a). The sequence alignment and probing are consistent with the possibility that H5 might, in most cases, be extended by two additional base pairs (G332–C314 and G333–C313, shown in dashed lines in Figs. 8 and 9). Extension of the anticodon stem is also possible in mitochondrial tRNAs (e.g., Okimoto & Wolstenholme, 1990) and in plant viral tRNA-like structures (e.g., Felden et al., 1994). In tmRNA, this implies that the position of the single-stranded RNA stretch U309–U312 could be in close proximity to the T-loop, perhaps mimicking the location of a D-loop. This region is conserved between the closely related species, but varies in length and sequence between the others (as do the D-loops of canonical tRNAs). Nevertheless, a guanosine is always present at 310 (capital letter in Fig. 5). Mimicry with a tRNA D-arm, as proposed previously (Felden et al., 1996a), is unclear, because of the questionable evidence for stem H2 (as noted above, covariation supports H2, but probing does not, so it may only form after a conformational change). Ushida et al. (1994) have proposed an alternate tRNA-like structure, in which a single-stranded RNA stretch, A8–A20, containing a GG doublet at similar location to the D-loop in tRNA, contributes to the tertiary folding of tmRNA. Despite several lead cleavages in this area, our probing data do not support A8–A20 being single-stranded, because of the strong V_1 cut between A8 and U12 and at C18, and the DMS and CMCT probing pattern (A8, C11–U12, G14, and G19–A20 are protected). A stem was also proposed between C21 and A25, and between U328 and G332 (in our case, H5 is made between A327 and C331 and between G315 and A319). Additional data, including a mutational analysis, are needed to discriminate between the two proposed stems at the 5′ side of the T-like stem H6.

In addition to the tRNA-like domain derived from juxtaposition of the 3′ and 5′ ends of tmRNA, there are two other recognizable structural units: the domain encompassing the coding sequence and a complex connecting unit that joins the tRNA-like domain to the coding sequence. This study suggests that the coding sequence is in two stem-loops, H3 and H4, and in the connecting 7-nt single-stranded stretch. It starts just before the loop closing H3 and ends in the loop closing H4. Thus, ribosomes would need to open up both stems. However, both proposed stems include unpaired nucleotides (A97 of H3 and U131 for H4), which would reduce their stability. An alternative folding of H3 can be proposed on the basis of sequence alignment (helix between U85 and G90, C95 and G90, C95 and A100, with an A96–G99 base pair, Fig. 5), but the probing data favor the slightly different folding proposed in Figures 8 and 9.

The connecting domain has pseudoknots, one on each side of the coding sequence, leading to the tRNA-like structure. The model poses that the three pseudoknots at the 3′ side of the coding sequence (PK2, PK3, and PK4) are connected to a sequence between R1 and PK1, via a possible long-range interaction, H2. The data indicate that the stability of PK1 and PK2 is low at 37 °C, perhaps in equilibrium between a closed and an opened conformation (Figs. 8 and 9 for details). The high density of pseudoknots connecting the two functional domains of tmRNA is striking. Pseudoknots are already known to play major roles in translation. Three pseudoknots are located within the 16S ribosomal RNA central core (Gutell et al., 1986), and pseudoknots in mRNAs are involved in recoding events (review, Brierley, 1995). Pseudoknot stretches are also found at the 3′ ends of several plant viral RNAs, connecting the very 3′ tRNA-like domain to the end of the coding sequence, but these tRNA-like structures are not involved in protein synthesis (for review, see Florentz & Giege, 1995). Despite some similar modular features, the overall structures are likely to be very different. In the case of tmRNA, it is possible that the proposed pseudoknots play a special role in positioning the tRNA-like domain and the coding sequence, so that the molecule can switch from a tRNA to an mRNA function. Analysis of the stem pK1.1, involving mutants of either strand that disrupt the stem and compensatory mutants that restore pairing, has provided direct support for both its existence and importance for translation (H. Himeno, N. Nameki, & A. Muto, unpubl.).

It is important to realize that this proposed structure is one that is consistent with most of the data, but certainly is not correct in detail. Clearly, alternate structures are possible, especially for tmRNA from organ-

isms that are distantly related to *E. coli*. It is hoped that this proposal for a folded structure of tmRNA will stimulate further experiments to better understand the structure and function of this interesting RNA.

MATERIALS AND METHODS

Chemicals and enzymes

DMS and imidazole were from Aldrich (Milwaukee, Wisconsin). Aniline, CMCT, DEPC, lead acetate, sodium borohydride, and hydrazine were from Sigma (St. Louis, Missouri). Nucleotides, deoxynucleotides, and dideoxynucleotides were from Pharmacia (Piscataway, New Jersey). Rotiphorese Gel 40 solution of acrylamide and *N, N'*-methylene-bis-acrylamide was from Bio-Rad (Hercules, California). Radioactive [^{32}P]pCp at 3,000 Ci/mol and [γ-^{32}P]ATP at 3,200 Ci/mol were from DuPont NEN (Wilmington, Delaware). Total yeast tRNA, used as a carrier RNA to supplement labeled RNA, was from Sigma. Nuclease-free water was from Promega (Madison, Wisconsin). Ribonucleases S_1, T_1, V_1, U_2, and alkaline phosphatase were from Pharmacia. Phage T4 polynucleotide kinase and T4 RNA ligase were from New England Biolabs (Beverly, Massachusetts).

Preparation of *E. coli* tmRNA and DNA oligonucleotides

A derivative of plasmid pGEMEX-2 with the *E. coli ssrA* gene expressed from T7 promoter was transformed into *E. coli* JM109 (DE3) that contains the T7 RNA polymerase gene driven from a *lac* promoter. tmRNA induced by the addition of 1 mM IPTG was purified as described (Ushida et al., 1994). This overproduction system yielded about a 100-fold higher amount of properly processed tmRNA, as shown by the ability to be aminoacylated with alanine in vitro.

Five synthetic DNA oligonucleotides, 5'-TGGTGGAGCT GGCGGGA-3', 5'-TTACATTCGCTTGCCAGC-3', 5'-CAGGC AGGGCTTCCACGC-3', 5'-GAGAGAGGGCTCTAAGCA-3', 5'-TTTTTACGAGGCCAACCG-3', complementary to residues C346–A363, G274–A291, G200–G217, U128–C145, and C56–A73, respectively, were prepared on an Applied Biosystems model 394 synthesizer using the phosphoramidite method.

Structural mapping procedures

Labeling at the 5'-end of tmRNA was performed with [γ-^{32}P]ATP and phage T4 polynucleotide kinase on RNA dephosphorylated previously with alkaline phosphatase (Silberklang et al., 1977). Labeling at the 3'-end was done by ligation of [γ-^{32}P]pCp using T4 RNA ligase (England & Uhlenbeck, 1978). After labeling, tmRNA is gel purified (10% PAGE), eluted, and ethanol precipitated. Before either enzymatic digestions or chemical modifications, the labeled tmRNA was heated to 75 °C for 3 min in the required buffers containing both monovalent and divalent cations, and cooled slowly at room temperature for 20 min. Cleavage or modification sites were detected by gel electrophoresis, either indirectly by analyzing DNA sequence patterns generated by primer extension upon reverse transcription of the modified RNAs, or by direct identification within the statistical cleavage patterns of the RNA itself.

Digestions with the various ribonucleases (V_1, S_1, T_1,) were performed as described (Felden et al., 1994) on both 3'- and 5'-labeled tmRNA (25,000–50,000 cpm/reaction, depending on the experiment), supplemented with 1 μg of total tRNA. The following amounts of nuclease were added: 6×10^{-2} units of RNase T_1, 0.3–0.4 units of RNase V_1, and 50–100 units of nuclease S_1. Incubation times were 7 min at the required temperature (20 °C, 37 °C, 42 °C, 46 °C, and 50 °C). Imidazole-induced cleavages of tmRNA were done as described (Vlassov et al., 1995), using an imidazole buffer at 0.8–1.6 M for a 13-h incubation time at 37 °C. Probing with lead acetate was performed as described (Krzyzosiak et al., 1988). Reactions were done in a 20-μL reaction volume at 37 °C for 5 min by addition of lead(II) acetate in final concentrations ranging from 0.7 to 1.3 mM. Reactions were stopped by addition of 1 μg carrier tRNA, 5 μL of 0.5 M EDTA, pH 8.2, and precipitated with ethanol.

Modification of N-3 atoms of cytosines and N-7 atoms of guanines by DMS, and of N-7 positions of adenines by DEPC were done at 37 °C according to Peattie and Gilbert (1980). Both the concentration of chemicals and the incubation times have been optimized and adapted from Felden et al. (1996b). Reaction mixtures contain the appropriate buffer, the labeled tmRNA (50,000 cpm) supplemented with 10 μg of total tRNA, 2–6 μL of diluted DMS solution (dilution of saturated stock solution was two-fold in 100% ethanol), or 5–15 μL of pure DEPC, depending on the experiment. Under both the native (with 20 mM magnesium acetate) and semi-denaturing conditions (supplemented with 1 mM EDTA and without magnesium), DMS modifications were done for 3–8 min. DEPC modifications were performed with 10–15 μL of pure DEPC for 10–30 min under native conditions, and with 5–7.5 μL under semi-denaturing conditions. Reactions were stopped and modifications or cleavage sites were assigned as described previously (Romby et al., 1987). Data were analyzed by phosphorimager. The background present in control lanes was substracted, but the quantitation of each fragment was scored manually.

TGGE experiments

TGGE experiments were performed essentially as described (Rosenbaum & Riesner, 1987; Henco et al., 1994). Native polyacrylamide gels (5%) containing 10 mM Tris-HCl, pH 7.4, 1 mM EDTA, and 5 mM $MgCl_2$ were set between one glass plate and a gel bond film from FMC bioproducts (Rockland, Maine). The hydrophobic side of the gel bond film was in contact with the glass plate, the hydrophilic side being covalently bound to the gel. The slot was 140 mm (perpendicular to the direction of the migration) $\times$ 5 mm. 3'-Labeled tmRNA (200,000 cpm) was loaded and electrophoresed into the matrix in the cold room at uniform temperature and low voltage. After 30–40 min of electrophoresis, the gel was placed onto a copper plate, establishing the temperature gradient, and covered with three 5-mm glass plates for thermal insulation. After starting the temperature gradient, the RNA was allowed to equilibrate for 10 min. tmRNA was then electrophoresed at low voltage (300 V) for 2.5 h.

ACKNOWLEDGMENTS

We thank Rafael Maldonado and Guido Grentzmann for help with the database searches and Christian Massire (Strasbourg, France) for examining the tmRNA sequences using computer-based secondary structure predictions. R.F.G. is an investigator of the Howard Hughes Medical Institute. This work was also supported by a grant (to J.F.A.) from the U.S. National Institutes of Health (RO1-GM48152) and by a Grant-in-Aid for the work in Hirosaki from the Ministry of Education, Science, and Culture, Japan.

Received October 4, 1996; returned for revision November 6, 1996; revised manuscript received November 8, 1996

REFERENCES

Atkins JF, Gesteland RF. 1996. A case for *trans translation*. *Nature 379*:769–771.

Brierley I. 1995. Ribosomal frameshifting on viral RNAs. *J Gen Virol 76*:1885–1892.

Brown JW, Hunt DK, Pace NR. 1990. Nucleotide sequence of the 10Sa RNA gene of the beta-purple eubacterium *Alcaligenes eutrophus*. *Nucleic Acids Res 18*:2820.

Brown RS, Hingerty BE, Dewan JC, Klug A. 1983. Pb(II)-catalysed cleavage of the sugar–phosphate backbone of yeast $tRNA^{Phe}$. Implications for lead toxicity and self-splicing RNA. *Nature 303*:543–546.

Chauhan AK, Apirion D. 1989. The gene for a small stable RNA (10Sa RNA) of *Escherichia coli*. *Mol Microbiol 3*:1481–1485.

England TE, Uhlenbeck OC. 1978. Enzymatic oligoribonucleotide synthesis with T4 RNA ligase. *Biochemistry 17*:2069–2076.

Felden B, Atkins JF, Gesteland RF. 1996a. tRNA and mRNA both in the same molecule. *Nature Structural Biol 3*:494.

Felden B, Florentz C, Giege R, Westhof E. 1994. Solution structure of the tRNA-like 3′-end of brome mosaic virus genomic RNAs. Conformational mimicry with canonical tRNAs. *J Mol Biol 235*:508–531.

Felden B, Florentz C, Giege R, Westhof E. 1996b. A central pseudoknotted three-way junction imposes tRNA-like mimicry and the orientation of three 5′ upstream pseudoknots in the 3′ terminus of tobacco mosaic virus RNA. *RNA 2*:201–212.

Fleischmann RD, Adams MD, White O, Clayton RA, Kirkness EF, Kerlavage AR, Bult CJ, Tomb JF, Dougherty BA, Merrick JM, McKenney K, Sutton G, Fitzhugh W, Fields C, Gocayne JD, Scott J, Shirley R, Liu LI, Glodek A, Kelley JM, Weidman JF, Phillips CA, Spriggs T, Hedblom E, Cotton MD, Utterback TR, Hanna MC, Nguyen DT, Saudek DM, Brandon RC, Fine LD, Fritchman JL, Fuhrmann JL, Geoghagen NSM, Gnehm CL, McDonald LA, Small KV, Fraser CM, Smith HO, Venter JC. 1995. Whole-genome random sequencing and assembly of *Haemophilus influenzae* Rd. *Science 269*:496–512.

Florentz C, Giege R. 1995. tRNA-like structures in viral RNAs. In: Söll D, RajBhandary UL, eds. *tRNA: Structure, biosynthesis and function*. Washington, DC: American Society of Microbiology. pp 141–163.

Francklyn C, Schimmel P. 1989. RNA minihelices can be aminoacylated with alanine. *Nature 337*:478–481.

Fraser CM, Gocayne JD, White O, Adams MD, Clayton RA, Fleischmann RD, Bult CJ, Kerlavage AR, Sutton G, Kelley JM, Fritchman JL, Weidman JF, Small KV, Sandusky M, Fuhrmann J, Nguyen D, Utterback TR, Suadek DM, Phillips CA, Merrick JM, Tomb JF, Dougherty BA, Bott KF, Hu PC, Lucier TS, Peterson SN, Smith HO, Hutchison CA III, Venter JC. 1995. The minimal gene complement of *Mycoplasma genitalium*. *Science 270*:397–403.

Gutell RR, Noller HF, Woese CR. 1986. Higher order structure in ribosomal RNA. *EMBO J 5*:1111–1113.

Henco K, Harders J, Wiese U, Riesner D. 1994. Temperature gradient gel electrophoresis (TGGE) for the detection of polymorphic DNA and RNA. *Methods Mol Biol 31*:211–228.

Jentsch S. 1996. When proteins receive deadly messages at birth. *Science 271*:955–956.

Keiler KC, Waller PRH, Sauer RT. 1996. Role of a peptide tagging system in degradation of proteins synthesized from damaged messenger RNA. *Science 271*:990–993.

Komine Y, Inokuchi H. 1991. Physical map locations of the genes that encode small stable RNAs in *Escherichia coli*. *J Bacteriol 173*:5252.

Komine Y, Kitabatake M, Yokogawa T, Nishikawa K, Inokuchi H. 1994. A tRNA-like structure is present in 10Sa RNA, a small stable RNA from *Escherichia coli*. *Proc Natl Acad Sci USA 91*:9223–9227.

Kovach ME. 1995. Identification and characterization of a *Vibrio cholerae* pathogenicity island that encodes environmentally regulated colonization determinants [thesis]. Shreveport, Louisiana: Louisiana State University Medical Center. [Genbank accession no. U39068].

Krzyzosiak WJ, Marciniec T, Wiewiorowski M, Romby P, Ebel JP, Giege R. 1988. Characterization of the lead(II)-induced cleavages in tRNAs in solution and effect of the Y-base removal in yeast $tRNA^{Phe}$. *Biochemistry 27*:5771–5777.

Lee SY, Baily SC, Apirion D. 1978. Small stable RNAs from *Escherichia coli*: Evidence for the existence of new molecules and for a new ribonucleoprotein particle containing 6S RNA. *J Bacteriol 133*:1015–1023.

Muto A, Sato M, Tadaki T, Fukushima M, Ushida C, Himeno H. 1996. Structure and function of 10Sa RNA: trans-translation system. *Biochimie*, in press.

Oh KK, Apirion D. 1991. 10Sa RNA, a small stable RNA of *Escherichia coli*, is functional. *Mol Gen Genet 229*:52–56.

Okimoto R, Wolstenholme DR. 1990. A set of tRNAs that lack either the TFC arm or the dihydrouridine arm: Towards a minimal tRNA adaptor. *EMBO J 9*:3405–3411.

Peattie DA, Gilbert W. 1980. Chemical probes for higher-order structure in RNA. *Proc Natl Acad Sci USA 77*:4679–4682.

Ray BK, Apirion D. 1979. Characterization of 10s RNA: A new stable RNA molecule from *Escherichia coli*. *Mol Gen Genet 174*:25–32

Romby P, Moras D, Dumas P, Ebel JP, Giege R. 1987. Comparison of the tertiary structure of yeast $tRNA^{Asp}$ and $tRNA^{Phe}$ in solution. Chemical modification study of the bases. *J Mol Biol 195*:193–204.

Rosenbaum V, Riesner D. 1987. Temperature-gradient gel electrophoresis. Thermodynamic analysis of nucleic acids and proteins in purified form and in cellular extracts. *Biophys Chem 26*:235–246.

Silberklang M, Prochiantz A, Haenni AL, Rajbhandary UL. 1977. Studies on the sequence of the 3′ terminal region of turnip yellow mosaic virus. *Eur J Biochem 72*:465–478.

ten Dam E, Pleij K, Draper D. 1992. Structural and functional aspects of RNA pseudoknots. *Biochemistry 31*:11665–11676.

Tu GF, Reid GE, Zhang JG, Moritz RL, Simpson RJ. 1995. C-terminal extension of truncated recombinant proteins in *Escherichia coli* with a 10Sa RNA decapeptide. *J Biol Chem 270*:9322–9326.

Tyagi JS, Kinger AK. 1992. Identification of the 10Sa RNA structural gene of *Mycobacterium tuberculosis*. *Nucleic Acids Res 20*:138.

Ushida C, Himeno H, Watanabe T, Muto A. 1994. tRNA-like structures in 10Sa RNAs of *Mycoplasma capricolum* and *Bacillus subtilis*. *Nucleic Acids Res 22*:3392–3396.

Vlassov VV, Zuber G, Felden B, Behr JP, Giege R. 1995. Cleavage of tRNA with imidazole and spermine imidazole constructs: A new approach for probing RNA structure. *Nucleic Acids Res 23*:3161–3167.

Werner C, Krebs B, Keith G, Dirheimer G. 1976. Specific cleavages of pure tRNAs by plumbous ions. *Biochim Biophys Acta 432*:161–175.